Title: Discovery of a Novel Inhibitor of Coronavirus 3CL Protease as a Clinical Candidate for the Potential Treatment of COVID-19

Short Title: Novel 3CL Protease Inhibitor for COVID-19

Authors: Britton Boras[1,†], Rhys M. Jones[1,†,*], Brandon J. Anson[9], Dan Arenson[4], Lisa Aschenbrenner[4], Malina A. Bakowski[11], Nathan Beutler[12], Joseph Binder[1], Emily Chen[11], Heather Eng[4], Jennifer Hammond[6], Robert Hoffman[1], Eugene P. Kadar[4], Rob Kania[1], Emi Kimoto[4], Melanie G. Kirkpatrick[11], Lorraine Lanyon[4], Emma K. Lendy[10], Jonathan R. Lillis[7], Suman A. Luthra[3], Chunlong Ma[8], Stephen Noell[4], R. Scott Obach[4], Matthew N. O' Brien[5], Rebecca O'Connor[4], Kevin Ogilvie[4], Dafydd Owen[3], Martin Pettersson[3], Matthew R Reese[4], Thomas F. Rogers[12,13], Michelle I. Rossulek[3], Jean G. Sathish[2], Claire Steppan[4], Martyn Ticehurst[7], Lawrence W. Updyke[3], Yuao Zhu[2], Jun Wang[8], Arnab K. Chatterjee[11]. Andrew D. Mesecar[9,10], Annaliesa S. Anderson[2], Charlotte Allerton[3]

Affiliations:

[1]Worldwide Research and Development, Pfizer Inc., La Jolla, CA 92121, [2]Pearl River, NY 10965, [3]Cambridge, MA 02139, [4]Groton, CT 06340, [5]Lake Forest, IL 60045, [6]Collegeville, PA 19426, USA, [7]Sandwich, CT13 9ND, UK

[8]Department of Pharmacology and Toxicology, College of Pharmacy, University of Arizona, Tucson, AZ, 85721

[9]Department of Biological Sciences, [10]Department of Biochemistry, Purdue University, West Lafayette, IN, 47907 USA.

[11]Calibr, a division of The Scripps Research Institute, La Jolla, CA 92037

[12]Department of Immunology and Microbiology, The Scripps Research Institute, La Jolla, CA 92037

[13]UC San Diego Division of Infectious Diseases and Global Public Health, UC San Diego School of Medicine, La Jolla, CA 92093.

† These authors contributed equally to this work.

* To whom correspondence should be addressed. Email: rhys.jones@pfizer.com

One Sentence Summary: The phosphate prodrug PF-07304814 is disclosed as an investigational novel intravenous small molecule 3CL protease inhibitor for COVID-19.

Abstract:

COVID-19 caused by the SARS-CoV-2 virus has become a global pandemic. 3CL protease is a virally encoded protein that is essential to the viral life cycle across a broad spectrum of coronaviruses with no close human analogs. The designed phosphate prodrug PF-07304814 is metabolized to PF-00835321 which is a potent inhibitor *in vitro* of the coronavirus family 3CL pro, with selectivity over human host protease targets. Furthermore, PF-00835231 exhibits potent *in vitro* antiviral activity against SARS-CoV-2 as a single agent and it is additive/synergistic in combination with remdesivir. We present the ADME, safety, and *in vitro* antiviral activity data to warrant clinical evaluation.

Main Text:

In December 2019, COVID-19 was identified as a new, potentially fatal, respiratory infection caused by severe acute respiratory syndrome coronavirus 2 (SARS-CoV-2) (*1*, *2*). Unlike previous coronavirus outbreaks that receded relatively quickly, the resultant COVID-19 pandemic spread across the globe. As of August 2020, over 24 million people have been infected and over 821,000 people have died globally with no approved drugs available to treat the disease (*3*).

The RNA-dependent RNA polymerase (RdRp) inhibitor remdesivir is currently undergoing clinical investigation for the treatment of SARS-CoV-2 and was granted emergency use authorization by the U.S. Food and Drug Administration (FDA) in May 2020 (*4*). To date, trials of remdesivir have shown significantly decreased recovery time for COVID-19 patients, but the drug has not had a significant effect on morbidity (*5*). Other classes of antivirals that exhibit single agent efficacy or that are complementary to remdesivir for use in combination regimens are essential to meet this substantial unmet need.

SARS-CoV-2 produces two large viral polyproteins, pp1a and pp1ab, which are processed by two virally encoded cysteine proteases, the main protease, also called 3C-like protease (3CL protease or 3CLpro) and the papain-like protease. Mutagenesis experiments with other coronaviruses have demonstrated that the activity of the 3CLpro is essential for viral replication (*6*, *7*). 3CLpro proteolytically processes the virus p1a/p1ab polyproteins at more than 10 junctions to generate a series of non-structural proteins critical for virus replication and transcription, including RdRp, the helicase, and the 3CLpro itself (*8*). No close human analogs of the coronavirus 3CLpro are known, suggesting that selective 3CLpro inhibitors should avoid unwanted polypharmacology (*9*). The essential functional importance of proteases in virus replication has led to the clinical success of protease inhibitors in combating both human immunodeficiency virus (HIV) and hepatitis C virus (HCV) (*10*–*13*). This together with the opportunity for selectivity, makes 3CLpro an attractive antiviral drug target (*14*).

Following the severe acute respiratory syndrome (SARS) outbreak in 2002-2003 we identified a potential small molecule protease inhibitor (PF-00835231) for the treatment of SARS-CoV,

using structure based drug design (*15*). Due to the SARS pandemic being brought under control in July 2003 following public health measures which incorporated patient isolation and travel restrictions, this project was discontinued. Given that the SARS-CoV and SARS-CoV-2 3CLpro sequences share 96% identity overall and 100% identity in the active site (*1*, *16*, *17*), following the emergence of SARS-CoV-2, PF-00835231 was identified as a potential SARS-CoV-2 3CLpro inhibitor for the treatment of COVID-19 disease.

Herein we describe the 3CLpro inhibitor, PF-00835231, and its novel phosphate prodrug, PF-07304814, and present broad-spectrum antiviral activity along with absorption, distribution, metabolism, excretion (ADME) and safety data highlighting its potential for the intravenous (IV) treatment of COVID-19 disease.

Results and Discussion

PF-00835231 exhibits tight and specific binding to SARS-CoV-2 3CL *in vitro*

Previously, it was shown that PF-00835231 potently inhibited SARS-CoV-2 3CLpro with a Ki value of 0.27±0.1nM (*15*). An X-ray co-crystal structure of PF-00835231 bound to SARS-CoV-2 3CLpro is consistent with PF-00835231 binding to the 3CLpro enzyme with a covalent and reversible interaction at the catalytic cysteine residue of the active site, thus inhibiting the activity of the 3CLpro (PDB-6XHM) (*15*). A thermal-shift assay was used to evaluate the direct binding between PF-00835231 and SARS-CoV-2 3CLpro. The melting temperature of SARS-CoV-2 3CLpro was shifted by 14.6℃ upon binding of PF-00835231, from 55.9±0.11℃ (n=16) to 70.5±0.12℃ (n=8). These data support tight and specific binding of PF-00835231 to SARS-

CoV-2 3CLpro (Fig. 1) and, thereby, provide further evidence for the molecular inhibitory mechanism of PF-00835231.

PF-00835231 has potent and broad-spectrum inhibitory activity against a panel of coronavirus 3CLpros

Since the active sites of 3CLpro are fairly well conserved across different coronaviruses, it was hypothesized that PF-00835231 could be active against other coronaviruses besides SARS-CoV (*15*, *18*). Consistent with this hypothesis, it was shown that PF-00835231 was also active against 3CLpros from SARS-CoV-2 and HCoV-229E (*15*). To further explore the notion that PF-00835231 could have pan-coronavirus activity, PF-00835231 was evaluated against 3CLpro from a variety of other coronaviruses representing alpha, beta and gamma groups of *Coronaviridae*, using biochemical Förster Resonance Energy Transfer (FRET) protease activity assays. PF-00835231 demonstrated potent inhibitory activity against all tested coronavirus 3CLpro including members of alpha-coronaviruses (NL63-CoV, PEDV, FIPV), beta-coronaviruses (HKU4-CoV, HKU5-CoV, HKU9-CoV, MHV-CoV, OC43-CoV, HKU1-CoV), and gamma-coronavirus (IBV-CoV), with Ki values, ranging from 30 pM to 4 nM (Table 1). The demonstrated activity is consistent with a potential therapeutic use against emerging coronaviruses. This inhibitory activity is restricted to coronavirus 3CLpros as PF-00835231 was inactive against a panel of human proteases and HIV protease (Table S1). PF-00835231 showed detectable activity against human cathepsin B but 1000-fold weaker affinity compared to 3CLpro (Table S1). Thereby, these data collectively support PF-00835231 is a selective *in vitro* protease inhibitor with broad coronavirus activity.

In vitro cellular antiviral activity of PF-00835231 against SARS-CoV-2

The antiviral activity of PF-00835231 against SARS-CoV-2 in cell culture was evaluated with a cytopathic effect (CPE) assay using either VeroE6 cells enriched for ACE2 (VeroE6-enACE2) receptor or VeroE6 cells constitutively expressing EGFP (VeroE6-EGFP). These cell lines were infected with the SARS-CoV-2 Washington strain 1 (WA1 - EPI_ISL_404895) or the BetaCoV GHB-03021/2020 strain (GHB-03021 - EPI_ISL_407976) (*19*), respectively, which have identical 3CLpro amino acid sequences. PF-00835231 exhibited viral CPE EC_{50} values of 39.7µM and 88.9µM, respectively (EC_{50}, Fig. 2). However, Vero cells express high levels of the efflux transporter P-glycoprotein (P-gp) (also known as MDR1 or ABCB1) (*20*), of which PF-00835231 is a known substrate (*15*) suggesting that the intracellular concentration of PF-00835231 was lower than the concentration added. Therefore, the assays were repeated in the presence of a P-gp efflux inhibitor, CP-100356 (*21*). PF-00835231 exhibited a 117- to 173-fold increase in activity in the presence of 2 µM P-gp inhibitor, with EC_{50} values of 0.23µM in VeroE6–enACE2 cells and 0.76µM in the VeroE6-EGFP cells (Fig. 2). The P-gp inhibitor alone had no antiviral or cytotoxic activity at these concentrations and did not cause cytotoxicity in the presence the protease inhibitor. Consistent with many viral protease inhibitors (*22*), there was a steep response to increasing doses of PF-00835231, with a ~2-3 fold difference between EC_{50} and EC_{90} in both cell types (EC_{90} = 0.48µM in VeroE6-enACE2 cells and EC_{90}= 1.6µM in VeroE6-EGFP cells in the presence of the P-gp inhibitor). When lung cell lines were tested for antiviral potency in the presence and absence of P-gp inhibitor (A549-ACE2 (*23*) and MRC5), no statistical difference in antiviral potency was observed (Fig. 2A). Additionally, antiviral activities in both VeroE6 cell lines with 2µM P-gp inhibitor are similar to those observed in more physiologically relevant human cell culture systems, including A549-ACE2 and polarized

human airway epithelial cells (*23*), where P-gp expression is lower. These data support the potential for single agent antiviral activity.

Potential for antiviral combination benefit of PF-00835231 in combination with remdesivir

Combinations of antiviral agents, especially those targeting different steps in the virus replication cycle, are a frequently employed therapeutic strategy in treating viral diseases (*24*). As PF-00835231 and remdesivir, a nucleoside RNA-dependent RNA polymerase inhibitor, target different steps in the virus replication cycle, the antiviral activity of the two compounds was evaluated alone and in combination using HeLa-ACE2 cells (*25*). Viral proteins were detected in this assay using convalescent human polyclonal sera from two different COVID-19 patients. PF-00835231 alone inhibited SARS-CoV-2 replication with an average EC_{50} of 0.14µM and EC_{90} of 0.40µM; whereas remdesivir had an average EC_{50} of 0.074µM and EC_{90} of 0.17µM (Fig. 3A). Combination studies were performed using a drug testing matrix, and the data for the drug combination were analyzed using reference models (Loewe, Bliss, HSA) to classify the effects of the drug combination as either additive, synergistic or antagonistic (isobologram, synergy scores, and combination indices).

As summarized in Fig. 3B, the combination of PF-00835231 and remdesivir exhibited synergy from patient #1 sera in 2 independent experiments and additivity in a single experiment with sera from patient #2 (Fig. 3B). The different classification is most likely due to the different convalescent serum used as detection reagents. These same antiviral data were also analysed using Synergyfinder, which also indicated that the 2 drugs were additive to synergistic, with a representative graph shown in Fig. 3B. Antagonism was not demonstrated for the combination of

PF-00835231 and remdesivir in these studies. The observed additivity/synergy was not due to cytotoxicity, as there was no noticeable cytotoxicity in virus infected host cells for all the combinations tested. This additivity/synergy is similar to other protease inhibitors used for the treatment of HCV which has led to substantial clinical benefit (*26*).

Favorable preclinical ADME and pharmacokinetic profile of PF-00835231

The metabolic stability of PF-00835231 was evaluated *in vitro* using pooled human liver microsomes (HLM). PF-00835231 was shown to be metabolized by cytochrome P450 enzymes exhibiting an unbound CL_{int} 14µl/min/mg. Using recombinant heterologously expressed enzymes and HLM with the CYP3A selective inhibitor ketoconazole, CYP3A4 was identified as the major CYP involved in the metabolism of PF-00835231. It was also noted that the polymorphically expressed CYP3A5 can also metabolize PF-00835231 and that clearance may be slightly greater in CYP3A5 expressers. The potential for PF-00835231 to reversibly inhibit human cytochrome P450 enzymes (CYP1A2, 2B6, 2C8, 2C9, 2C19, 2D6, and 3A) was evaluated using probe substrates in pooled HLM and provided IC_{50} values >200 µM and a weak signal for time dependent inhibition (TDI) of CYP3A4/5. These data indicate PF-00835231 provides a low risk of causing drug-drug interactions (DDIs) on coadministration with other drugs. The potential for PF-00835231 to inhibit a range of transporters (BCRP, P-gp, OATP1B1/1B3, OCT1/2, OAT1/3 and MATE1/2K) was evaluated using *in vitro* systems. The IC_{50} values were >20µM and indicate a low risk of causing DDIs due to transporter inhibition at the projected clinical exposure. The plasma protein binding of PF-00835231 was measured across species using equilibrium dialysis and demonstrated moderate binding to plasma proteins with plasma free fractions of 0.33 to 0.45 across species.

PF-00835231 was administered IV to rats, dogs and monkeys (1 or 2mg/kg) and exhibited moderate plasma clearances (50-80% liver blood flow), low volumes of distribution (<1.5 L/kg) and short half-lives (<2 hours) across species in keeping with its lipophilic ($LogD_{7.4}$=1.7) and neutral physicochemistry. Following oral administration to rats (2 mg/kg) and monkeys (5 mg/kg) PF-00835231 exhibited low oral bioavailability (<2%), likely due to a combination of low absorption because of its low permeability (apparent MDCK-LE permeability of $1.3x10^{-6}$cm/sec(*27*, *28*), low solubility, potential for active efflux in the gut by P-gp and BCRP, and the potential for amide hydrolysis by digestive enzymes in the gastrointestinal tract. In rat, dog and monkey approximately 10% or less of PF-00835231 was eliminated unchanged in the urine indicating renal elimination may also play a minor role in the clearance of PF-00835231 in humans. Additional data presented in the supplementary data (Tables S1-S7).

Human pharmacokinetic predictions suitable for IV administration

Taking into account the human *in vitro* metabolism data and *in vivo* pharmacokinetic (PK) data in rats, dogs and monkeys, PF-00835231 was predicted to exhibit a plasma clearance (CL_p) of ~6mL/min/kg (major CYP, minor renal pathways), steady state volume of distribution (V_{dss}) of 1L/kg and half-life of approximately 2 hours in humans. Due to the limited oral bioavailability, short elimination half-life, and the likely need to maintain free systemic concentrations over time to achieve antiviral activity, a continuous IV infusion was proposed as the optimal dosing route and regimen.

Efficacious target concentration and feasible human dose projection

The projected minimally efficacious concentration (C_{eff}) was chosen to match the *in vitro* EC_{90} (please see supplemental methods for rationale), consistent with the preclinical to clinical translation of approved protease inhibitors (*29*). Since PF-00835231 was proposed to be administered by continuous infusion, the projected steady-state exposure is equal to the C_{min} maintained over the dosing interval. The dose response assay performed in the most physiologically relevant cell type, human lung carcinoma, resulted in an average EC_{90} value of 0.44μM (*23*). This is consistent with additional antiviral data in Hela-ACE2 cells (EC_{90}=0.4μM) and Vero cell lines (EC_{90}= 0.48-1.6μM) when a P-gp inhibitor was added to better reflect the lack of substantial P-gp transporter in the lung (Fig. 2B). Furthermore, the antiviral inhibition is supported by the antiviral time course experiment performed in a primary human airway epithelial model (preliminary data indicates an unbound EC_{90} <0.5 μM) (*23*), indicating a consistent intrinsic anti-SARS-CoV-2 activity of PF-00835231 across different cell types. Therefore, the proposed minimal C_{eff} is ~0.5μM.

Due to the rapid blood perfusion through the lungs and the continuous steady state intravenous infusion regimen, the free plasma and free lung concentrations are assumed to be in equilibrium and, therefore, the free plasma concentration provides a reasonable surrogate for the concentration at the main site of action of the disease. Based on the human PK predictions, the minimally efficacious dose of PF-00835231 necessary to achieve this exposure is ~320 mg/day administered as an intravenous continuous infusion. The required duration of dosing for efficacy remains uncertain and will need to be evaluated in humans. Based on clinical results from

remdesivir a duration of up to 10 days of dosing may be required to provide improved patient outcomes (*5*).

Formulation and solubility profile of PF-00835231 to enable IV administration

PF-00835231 is a moderately lipophilic ($LogD_{7.4}$ = 1.7), neutral molecule with no ionizable centers throughout the physiologically relevant pH range. Consequently, PF-00835231 exhibits a pH independent solubility with an intrinsic aqueous solubility of less than 0.1mg/mL and limited opportunities for solubility-enabling formulation approaches. Preliminary work using standard solubilizing excipients indicated that achieving a solubility >0.5mg/mL would likely be challenging.

Based on a maximum desired intravenous infusion volume of ~1L per day a solubility of 0.5mg/mL would be sufficient to deliver the minimal efficacious dose estimate of ~320 mg/day to maintain a ~0.5µM steady state unbound concentration (Fig. 4B). Due to the nascent understanding of the virus and the current lack of *in vivo* data to aid clinical translation, the required target levels of inhibition for clinical benefit remain uncertain and the ability to evaluate exposures up to ~10x C_{eff} in early clinical development is desirable. As a potential option to increase exposures, and/or decrease the required infusion volume, the use of a strong CYP3A inhibitor (itraconazole 200mg QD for 15 days) was considered but preliminary, physiologically-based pharmacokinetic (PBPK) modeling predicted only a ~2-fold increase in PF-00835231 exposure at steady state (supplemental Table S10).

The ability to achieve higher doses could also potentially mitigate a higher than predicted clearance, or variations in patient body weight. Therefore, a medicinal chemistry strategy to significantly enhance the aqueous solubility of PF-00835231, by designing a phosphate prodrug was pursued.

Considering an intravenous phosphate prodrug approach to improve solubility

IV phosphate prodrugs have precedence with several commercially available drugs such as fosfluconazole and fosphenytoin which are rapidly cleaved by human alkaline phosphatase to provide high systemic exposures of their respective active moieties following IV administration (Fig. 4) (*30*, *31*). Alkaline phosphatase is ubiquitously expressed across tissues with high levels expressed in the liver, lung, and kidney (ALPL tissue data from v19.proteinatlas.org (*32*)). High levels of conversion from prodrug to active moiety for fosfluconazole and fosphenytoin have also been observed in rats and dogs supporting cross species translation to human for the conversion of prodrug to active moiety (*31*, *33*). Overall, the use of a phosphate prodrug is an established approach for IV administration to provide rapid conversion to its active moiety and was considered for PF-00835231.

Synthetic route to provide phosphate prodrug

The synthesis of PF-00835231 has been described previously (*15*). The subsequent synthesis of the phosphate prodrug of PF-00835231 was achieved via two steps (Fig. S1). Briefly, treatment of **1** (PF-00835231) with di-*tert*-butyl *N*,*N*-dipropan-2-ylphosphoramidite and tetrazole in tetrahydrofuran followed by oxidation with aqueous hydrogen peroxide delivered intermediate **2**.

The phosphate *t*-butyl groups were subsequently hydrolyzed using trifluoroacetic acid in dichloromethane to deliver phosphate prodrug **3** (PF-07304814) as a solid.

Enhanced formulation and solubility profile of PF-07304814 to provide clinical flexibility

PF-07304814 rapidly undergoes *in vivo* conversion to the active metabolite PF-00835231 (Fig. 3A). The phosphate prodrug is weakly acidic, with pKas of 1 and 6.4, and a predicted $LogD_{7.4}$ of -3.7. At pHs above the compound's first pKa, the phosphate functional group is de-protonated and negatively charged, which enables a significant improvement in aqueous solubility to greater than 200mg/mL over a pH range compatible with intravenous infusion. The higher intrinsic solubility of PF-07304814 eliminates the need for solubility-enabling formulations and enables the use of standard IV compatible excipients. Furthermore, the improved solubility enables higher doses to be explored in the clinic and gives clinicians greater flexibility in terms of dose volume to account for patient-specific co-administration requirements.

PF-07304814 (prodrug) preclinical *in vitro* and *in vivo* ADME profile

To understand the metabolic stability and conversion of PF-07304814 to its active moiety (PF-00835231), PF-07304814 enzyme kinetics were evaluated *in vitro* using liver S9 fractions and was shown to exhibit rapid conversion to PF-00835231 with unbound CL_{int} values of 51, 84, 168 and 428µl/min/mg in rat, dog, monkey and human respectively. In these *in vitro* systems, PF-00835231 was the only metabolite formed from PF-07304814. Conversion was rapid in phosphate-free incubations but abolished in the presence of phosphate buffer supporting the role of alkaline phosphatase in this conversion (Table S8, Fig. S2). To evaluate the *in vivo* conversion

and systemic availability of the active moiety PF-00835231, PF-07304814 was administered intravenously to rats, dogs and monkeys. PF-07304814 exhibited high systemic clearance and short half-life across species forming 68, 81, 76% PF-00835231 in rats, dogs and monkey respectively in comparison to the systemic exposure achieved with IV administration of PF-00835231 (Fig. 5A).

PF-07304814 was also evaluated for the potential to cause reversible and time dependent inhibition of human cytochrome P450 enzymes using pooled HLM and probe substrates for a range of CYP enzymes (CYP1A2, 2C8, 2C9, 2C19, 2D6, and 3A4/5) and showed low risk with IC_{50} values >100µM and no evidence of TDI. The potential for PF-07304814 to inhibit a range of transporters (BCRP, P-gp, OATP1B1/1B3, OCT1/2, OAT1/3 and MATE1/2K) was evaluated using *in vitro* systems providing IC_{50} values >130µM indicating a low risk of causing DDIs due to transporter inhibition at the projected C_{eff}. The plasma protein binding of PF-07304814 was measured across species using equilibrium dialysis showing moderate binding to plasma proteins with plasma free fractions of 0.18 to 0.38 across species. Additional data presented in the supplementary data (Tables S3, S5-S7).

Encouraging human PK predictions for PF-00835231 formation

The predicted human plasma clearance of PF-07304814 is ~10mL/min/kg based on scaling *in vitro* human liver S9 CL_{int} data (using equations 9 and 10, see Methods) and represents a conservative prediction of total Cl_p as it only accounts for conversion of prodrug to active moiety in the liver. The human Vd_{ss} for PF-07304814 is predicted to be ~0.1L/kg based on its acidic physiochemistry and observed human Vd_{ss} values of other phosphate prodrugs (*30*, *31*). Based

on the predicted Cl_p, Vd_{ss}, and a ~75% conversion to PF-00835231 based on the mean conversion in animals, PF-07304814 is anticipated to exhibit a short half-life of ~0.1hour with high conversion to the active moiety (Fig. 5B).

PF-07304814 unlikely to contribute to antiviral activity *in vivo*

In a direct comparison, using the same SARS-Cov-2 3CLpro assay method as described in (*15*), the prodrug PF-07304814 binds and inhibits SARS-CoV-2 3CLpro activity with a Ki of 174nM providing a >600-fold higher Ki in comparison to the active moiety PF-00835231 (0.27nM) (*15*). However, PF-07304814 shows similar antiviral activity to PF-00835231 (1-12-fold, Fig. 2A) across cellular *in vitro* assays, most likely due to the partial conversion of PF-07304814 to PF-00835231 in the cellular assays by alkaline phosphatase. This was consistent with PF-00835231 concentrations measured at approximately 50% of the PF-07304814 starting concentration at the end of the 3-day incubation in the VeroE6 cell assay.

PF-07304814 dose projection provides clinical flexibility to achieve target C_{eff}

The antiviral activity for PF-00835231 was used to derive the minimal C_{eff} and dose estimates. Based on the predicted human PK and 75% conversion of the prodrug, a free plasma concentration of the active moiety PF-00835231 of 0.5µM (C_{eff}) can be achieved with a 500 mg continuous IV infusion of the prodrug over 24 hours (Fig. 5C). The estimated time to achieve 90% steady state exposure of PF-00835231 is approximately 6 hours. Due to the improved solubility (>200mg/mL), the dose of PF-0730814 can be delivered in a volume of less than 0.25L. In addition the dose can be increased if the observed human plasma Cl exceeds

6mL/min/kg, if the percent converted from prodrug to active is less than predicted, or if exposures in excess of the minimal C_{eff} (0.5µM) are required to maximize clinical activity (Fig. 4B). Overall the improved solubility would theoretically enable >100-fold the proposed minimal C_{eff} dose in a 0.25L dose volume.

Preclinical safety profile supports progression to clinical evaluation

A toxicology assessment consisting of an *in vitro* battery of genetic toxicity, secondary and safety pharmacology studies, in conjunction with a single species (rat) *in vivo* Good Laboratory Practice (GLP) study has been completed. Data from repeat dose toxicology studies in rodent and non-rodent are planned or currently underway.

The safety profiles of PF-07304814 and PF-00835231 were assessed individually in a range of *in vitro* and *in vivo* safety studies in rats. In the *in vitro* studies, PF-07304814 and PF-00835231 were negative in the bacterial reverse mutation assay and did not induce micronuclei formation. Both compounds had minimal potential for secondary (off-target) pharmacology at clinically relevant exposures. Neither PF-07304814 nor PF-00835231 inhibited hERG current amplitude at up to 300µM (1,770- and 600-fold, respectively, in reference to the projected unbound human C_{max} of 0.17 and 0.50µM, respectively, at the projected human efficacious dose), indicating a favorable cardiovascular safety profile. In human blood hemocompatibility assays, both compounds had no effect on hemolysis or flocculation/turbidity parameters, indicating compatibility with human blood and supporting intravenous administration.

PF-07304814 was administered to rats via continuous IV infusion for 24 hours in a GLP study. There were no test article related findings and no target organ toxicity was identified. PF-07304814 had no effects on neurological safety pharmacology parameters as assessed by functional observation battery in the 24-hour continuous IV infusion rat study. The no observed adverse effect level (NOAEL) was 1000mg/kg. PF-00835231 was also administered to male rats via continuous IV infusion for 4 days in a non-GLP exploratory toxicity study and was tolerated at 246mg/kg/day, the highest feasible dose tested. PF-00835231-related findings in this study were limited to minimal, non-adverse effects on clinical chemistry parameters including higher mean triglycerides (1.9-3.6x vs controls), cholesterol (1.3x), and phosphorus (1.1x) without any microscopic correlates or associated functional changes. No test article related adverse effects were seen in any study.

At the NOAEL from the 24-hour, GLP continuous IV infusion study with PF-07304814 in rats, the anticipated exposure margins for unbound C_{max} and AUC_{24} are 97 and 65-fold for PF-07304814 and 25 and 21-fold for PF-00835231, at the projected minimum human efficacious dose of 500mg/day. This indicates the potential to safely evaluate multiples over EC_{90} in humans during clinical testing to understand the exposure response relationship and to achieve high levels of inhibition, if required. Furthermore, no overlapping or additive toxicity with medications currently being used in standard of care COVID-19 treatment is expected with administration of PF-07304814 in humans, making PF-07304814 an attractive combination partner. Based on results from the set of safety studies conducted, PF-07304814 exhibited an encouraging nonclinical safety profile and supported progression into Phase 1 clinical studies.

Conclusions

PF-07304814 is a phosphate prodrug that is rapidly converted *in vivo* to the active moiety, PF-00835231, which exhibits high selectivity over human proteases and acts as a broad-spectrum coronavirus 3CL protease inhibitor. Robust antiviral activity was demonstrated in a range of cellular *in vitro* assays in keeping with SARS-COV-2 human airway epithelial data (*23*) suggesting a C_{eff} value of ~0.5μM. The predicted human pharmacokinetics of PF-07304814 provide the ability to achieve systemic unbound concentrations of 0.5μM (EC_{90}) of PF-00835231 by delivering 500mg as a continuous infusion over 24 hours with infusion volumes of less than 0.25L. In addition, higher doses (up to and beyond 10x C_{eff}) also remain feasible if needed due to the high solubility of PF-07304814.

Overall, PF-07304814 exhibits an encouraging preclinical profile that has the SARS-CoV-2 antiviral activity, ADME, and safety profile that supports progression to the clinic as a potential novel COVID-19 single agent antiviral treatment, with potential for further additional benefit in combination with antivirals that target other critical stages of the coronavirus life cycle. The favorable profile of PF-07304814 warrants clinical evaluation.

References and Notes

1. P. Zhou, X.-L. Yang, X.-G. Wang, B. Hu, L. Zhang, W. Zhang, H.-R. Si, Y. Zhu, B. Li, C.-L. Huang, H.-D. Chen, J. Chen, Y. Luo, H. Guo, R.-D. Jiang, M.-Q. Liu, Y. Chen, X.-R. Shen, X. Wang, X.-S. Zheng, K. Zhao, Q.-J. Chen, F. Deng, L.-L. Liu, B. Yan, F.-X. Zhan, Y.-Y. Wang, G.-F. Xiao, Z.-L. Shi, A pneumonia outbreak associated with a new coronavirus of probable bat origin. *Nature*. **579**, 270–273 (2020).

2. A. R. Sahin, 2019 Novel Coronavirus (COVID-19) Outbreak: A Review of the Current Literature. *Eurasian J. Med. Oncol.* (2020), doi:10.14744/ejmo.2020.12220.

3. WHO Coronavirus Disease (COVID-19) Dashboard, (available at https://covid19.who.int).

4. "Coronavirus (Covid-19) Update: FDA Issues Emergency Use Authorization for Potential Covid-19 Treatment" (FDA, 2020), (available at https://www.fda.gov/news-events/press-announcements/coronavirus-covid-19-update-fda-issues-emergency-use-authorization-potential-covid-19-treatment).

5. J. H. Beigel, K. M. Tomashek, L. E. Dodd, A. K. Mehta, B. S. Zingman, A. C. Kalil, E. Hohmann, H. Y. Chu, A. Luetkemeyer, S. Kline, D. Lopez de Castilla, R. W. Finberg, K. Dierberg, V. Tapson, L. Hsieh, T. F. Patterson, R. Paredes, D. A. Sweeney, W. R. Short, G. Touloumi, D. C. Lye, N. Ohmagari, M.-D. Oh, G. M. Ruiz-Palacios, T. Benfield, G. Fätkenheuer, M. G. Kortepeter, R. L. Atmar, C. B. Creech, J. Lundgren, A. G. Babiker, S. Pett, J. D. Neaton, T. H. Burgess, T. Bonnett, M. Green, M. Makowski, A. Osinusi, S. Nayak, H. C. Lane, ACTT-1 Study Group Members, Remdesivir for the Treatment of Covid-19 - Preliminary Report. *N. Engl. J. Med.* (2020), doi:10.1056/NEJMoa2007764.

6. J. C. Kim, R. A. Spence, P. F. Currier, X. Lu, M. R. Denison, Coronavirus protein processing and RNA synthesis is inhibited by the cysteine proteinase inhibitor E64d. *Virology*. **208**, 1–8 (1995).

7. C. C. Stobart, A. S. Lee, X. Lu, M. R. Denison, Temperature-sensitive mutants and revertants in the coronavirus nonstructural protein 5 protease (3CLpro) define residues involved in long-distance communication and regulation of protease activity. *J. Virol.* **86**, 4801–4810 (2012).

8. A. Hegyi, J. Ziebuhr, Conservation of substrate specificities among coronavirus main proteases. *J. Gen. Virol.* **83**, 595–599 (2002).

9. K. Anand, J. Ziebuhr, P. Wadhwani, J. R. Mesters, R. Hilgenfeld, Coronavirus Main Proteinase (3CLpro) Structure: Basis for Design of Anti-SARS Drugs. *Science*. **300**, 1763–1767 (2003).

10. B. R. Bacon, S. C. Gordon, E. Lawitz, P. Marcellin, J. M. Vierling, S. Zeuzem, F. Poordad, Z. D. Goodman, H. L. Sings, N. Boparai, M. Burroughs, C. A. Brass, J. K. Albrecht, R. Esteban, Boceprevir for Previously Treated Chronic HCV Genotype 1 Infection. *N. Engl. J. Med.* **364**, 1207–1217 (2011).

11. A. Chary, M. Holodniy, Recent Advances in Hepatitis C Virus Treatment: Review of HCV Protease Inhibitor Clinical Trials. *Rev. Recent Clin. Trials*. **5**, 158–173 (2010).

12. R. M. W. Hoetelmans, C. H. W. Koks, J. H. Beijnen, P. L. Meenhorst, J. W. Mulder, D. M. Burger, Clinical pharmacology of HIV protease inhibitors: focus on saquinavir, indinavir, and ritonavir. *Pharm. World Sci.* **19**, 159–175 (1997).

13. Z. Lv, Y. Chu, Y. Wang, HIV protease inhibitors: a review of molecular selectivity and toxicity. *HIVAIDS Auckl. NZ.* **7**, 95–104 (2015).

14. T. Pillaiyar, M. Manickam, V. Namasivayam, Y. Hayashi, S.-H. Jung, An Overview of Severe Acute Respiratory Syndrome–Coronavirus (SARS-CoV) 3CL Protease Inhibitors: Peptidomimetics and Small Molecule Chemotherapy. *J. Med. Chem.* **59**, 6595–6628 (2016).

15. R. Hoffman, R. S. Kania, M. A. Brothers, J. F. Davies, R. A. Ferre, K. S. Gajiwala, M. He, R. J. Hogan, K. Kozminski, L. Y. Li, J. W. Lockner, J. Lou, M. T. Marra, L. J. M. J. Mitchell Jr, B. W. Murray, J. A. Nieman, S. Noell, S. P. Planken, T. Rowe, K. Ryan, G. J. Smith III, J. E. Solowiej, C. M. Steppan, B. Taggart, The Discovery of Ketone-Based Covalent Inhibitors of Coronavirus 3CL Proteases for the Potential Therapeutic Treatment of COVID-19 (2020), doi:10.26434/chemrxiv.12631496.v1.

16. M. A. Marra, S. J. M. Jones, C. R. Astell, R. A. Holt, A. Brooks-Wilson, Y. S. N. Butterfield, J. Khattra, J. K. Asano, S. A. Barber, S. Y. Chan, A. Cloutier, S. M. Coughlin, D. Freeman, N. Girn, O. L. Griffith, S. R. Leach, M. Mayo, H. McDonald, S. B. Montgomery, P. K. Pandoh, A. S. Petrescu, A. G. Robertson, J. E. Schein, A. Siddiqui, D. E. Smailus, J. M. Stott, G. S. Yang, F. Plummer, A. Andonov, H. Artsob, N. Bastien, K. Bernard, T. F. Booth, D. Bowness, M. Czub, M. Drebot, L. Fernando, R. Flick, M. Garbutt, M. Gray, A. Grolla, S. Jones, H. Feldmann, A. Meyers, A. Kabani, Y. Li, S. Normand, U. Stroher, G. A. Tipples, S. Tyler, R. Vogrig, D. Ward, B. Watson, R. C. Brunham, M. Krajden, M. Petric, D. M. Skowronski, C. Upton, R. L. Roper, The Genome Sequence of the SARS-Associated Coronavirus. *Science*. **300**, 1399–1404 (2003).

17. P. A. Rota, M. S. Oberste, S. S. Monroe, W. A. Nix, R. Campagnoli, J. P. Icenogle, S. Peñaranda, B. Bankamp, K. Maher, M. Chen, S. Tong, A. Tamin, L. Lowe, M. Frace, J. L. DeRisi, Q. Chen, D. Wang, D. D. Erdman, T. C. T. Peret, C. Burns, T. G. Ksiazek, P. E. Rollin, A. Sanchez, S. Liffick, B. Holloway, J. Limor, K. McCaustland, M. Olsen-Rasmussen, R. Fouchier, S. Günther, A. D. M. E. Osterhaus, C. Drosten, M. A. Pallansch, L. J. Anderson, W. J. Bellini, Characterization of a Novel Coronavirus Associated with Severe Acute Respiratory Syndrome. *Science*. **300**, 1394–1399 (2003).

18. L. Zhang, D. Lin, X. Sun, U. Curth, C. Drosten, L. Sauerhering, S. Becker, K. Rox, R. Hilgenfeld, Crystal structure of SARS-CoV-2 main protease provides a basis for design of improved α-ketoamide inhibitors. *Science*. **368**, 409–412 (2020).

19. S. Elbe, G. Buckland-Merrett, Data, disease and diplomacy: GISAID's innovative contribution to global health. *Glob. Chall. Hoboken NJ.* **1**, 33–46 (2017).

20. M. F. D. Rosa, D. Sillence, C. Ackerley, C. Lingwood, Role of Multiple Drug Resistance Protein 1 in Neutral but Not Acidic Glycosphingolipid Biosynthesis. *J. Biol. Chem.* **279**, 7867–7876 (2004).

21. A. S. Kalgutkar, K. S. Frederick, J. Chupka, B. Feng, S. Kempshall, R. J. Mireles, K. S. Fenner, M. D. Troutman, N-(3,4-dimethoxyphenethyl)-4-(6,7-dimethoxy-3,4-dihydroisoquinolin-2[1H]-yl)-6,7-dimethoxyquinazolin-2-amine (CP-100,356) as a "chemical knock-out equivalent" to assess the impact of efflux transporters on oral drug absorption in the rat. *J. Pharm. Sci.* **98**, 4914–4927 (2009).

22. L. Shen, S. Peterson, A. R. Sedaghat, M. A. McMahon, M. Callender, H. Zhang, Y. Zhou, E. Pitt, K. S. Anderson, E. P. Acosta, R. F. Siliciano, Dose-response curve slope sets class-specific limits on inhibitory potential of anti-HIV drugs. *Nat. Med.* **14**, 762–766 (2008).

23. M. de Vries, A. S. Mohamed, R. A. Prescott, A. M. Valero-Jimenez, L. Desvignes, R. O'Connor, C. Steppan, A. S. Anderson, J. Binder, M. Dittmann, *bioRxiv*, in press, doi:10.1101/2020.08.28.272880.

24. P. Erb, M. Battegay, W. Zimmerli, M. Rickenbach, M. Egger, Effect of Antiretroviral Therapy on Viral Load, CD4 Cell Count, and Progression to Acquired Immunodeficiency Syndrome in a Community Human Immunodeficiency Virus–Infected Cohort. *Arch. Intern. Med.* **160**, 1134–1140 (2000).

25. M. A. Bakowski, N. Beutler, E. Chen, T.-T. H. Nguyen, M. G. Kirkpatrick, M. Parren, L. Yang, J. Ricketts, A. K. Gupta, M. V. Hull, P. G. Schultz, D. R. Burton, A. K. Chatterjee, C. W. McNamara, T. F. Rogers, *bioRxiv*, in press, doi:10.1101/2020.06.16.153403.

26. Y. Koizumi, H. Ohashi, S. Nakajima, Y. Tanaka, T. Wakita, A. S. Perelson, S. Iwami, K. Watashi, Quantifying antiviral activity optimizes drug combinations against hepatitis C virus infection. *Proc. Natl. Acad. Sci. U. S. A.* **114**, 1922–1927 (2017).

27. L. Di, C. Whitney-Pickett, J. P. Umland, H. Zhang, X. Zhang, D. F. Gebhard, Y. Lai, J. J. Federico, R. E. Davidson, R. Smith, E. L. Reyner, C. Lee, B. Feng, C. Rotter, M. V. Varma, S. Kempshall, K. Fenner, A. F. El-kattan, T. E. Liston, M. D. Troutman, Development of a new permeability assay using low-efflux MDCKII cells. *J. Pharm. Sci.* **100**, 4974–4985 (2011).

28. M. V. Varma, I. Gardner, S. J. Steyn, P. Nkansah, C. J. Rotter, C. Whitney-Pickett, H. Zhang, L. Di, M. Cram, K. S. Fenner, A. F. El-Kattan, pH-Dependent solubility and permeability criteria for provisional biopharmaceutics classification (BCS and BDDCS) in early drug discovery. *Mol. Pharm.* **9**, 1199–1212 (2012).

29. M. B. Reddy, P. N. Morcos, S. Le Pogam, Y. Ou, K. Frank, T. Lave, P. Smith, Pharmacokinetic/Pharmacodynamic Predictors of Clinical Potency for Hepatitis C Virus Nonnucleoside Polymerase and Protease Inhibitors. *Antimicrob. Agents Chemother.* **56**, 3144–3156 (2012).

30. S. Sobue, K. Tan, G. Layton, M. Eve, J. B. Sanderson, Pharmacokinetics of fosfluconazole and fluconazole following multiple intravenous administration of fosfluconazole in healthy male volunteers. *Br. J. Clin. Pharmacol.* **58**, 20–25 (2004).

31. V. J. Stella, A case for prodrugs: Fosphenytoin. *Adv. Drug Deliv. Rev.* **19**, 311–330 (1996).

32. M. Uhlén, L. Fagerberg, B. M. Hallström, C. Lindskog, P. Oksvold, A. Mardinoglu, Å. Sivertsson, C. Kampf, E. Sjöstedt, A. Asplund, I. Olsson, K. Edlund, E. Lundberg, S. Navani, C. A.-K. Szigyarto, J. Odeberg, D. Djureinovic, J. O. Takanen, S. Hober, T. Alm, P.-H. Edqvist, H. Berling, H. Tegel, J. Mulder, J. Rockberg, P. Nilsson, J. M. Schwenk, M. Hamsten, K. von Feilitzen, M. Forsberg, L. Persson, F. Johansson, M. Zwahlen, G. von

Heijne, J. Nielsen, F. Pontén, Tissue-based map of the human proteome. *Science*. **347** (2015), doi:10.1126/science.1260419.

33. T. Aoyama, K. Ogata, M. Shimizu, S. Hatta, K. Masuhara, Y. Shima, K. Kimura, Y. Matsumoto, Pharmacokinetics of Fluconazole and Fosfluconazole after intraperitoneal administration to peritoneal dialysis rats. *Drug Metab. Pharmacokinet.* **20**, 485–490 (2005).

34. Broad-spectrum inhibition of coronavirus main and papain-like proteases by HCV drugs (2020), doi:10.21203/rs.3.rs-26344/v1.

35. A. K. Ghosh, K. Xi, K. Ratia, B. D. Santarsiero, W. Fu, B. H. Harcourt, P. A. Rota, S. C. Baker, M. E. Johnson, A. D. Mesecar, Design and Synthesis of Peptidomimetic Severe Acute Respiratory Syndrome Chymotrypsin-like Protease Inhibitors. *J. Med. Chem.* **48**, 6767–6771 (2005).

36. V. Grum-Tokars, K. Ratia, A. Begaye, S. C. Baker, A. D. Mesecar, Evaluating the 3C-like protease activity of SARS-Coronavirus: Recommendations for standardized assays for drug discovery. *Virus Res.* **133**, 63–73 (2008).

37. S. Tomar, M. L. Johnston, S. E. St John, H. L. Osswald, P. R. Nyalapatla, L. N. Paul, A. K. Ghosh, M. R. Denison, A. D. Mesecar, Ligand-induced Dimerization of Middle East Respiratory Syndrome (MERS) Coronavirus nsp5 Protease (3CLpro): IMPLICATIONS FOR nsp5 REGULATION AND THE DEVELOPMENT OF ANTIVIRALS. *J. Biol. Chem.* **290**, 19403–19422 (2015).

38. S. E. St John, S. Tomar, S. R. Stauffer, A. D. Mesecar, Targeting zoonotic viruses: Structure-based inhibition of the 3C-like protease from bat coronavirus HKU4--The likely reservoir host to the human coronavirus that causes Middle East Respiratory Syndrome (MERS). *Bioorg. Med. Chem.* **23**, 6036–6048 (2015).

39. S. Agnihothram, B. L. Yount, E. F. Donaldson, J. Huynh, V. D. Menachery, L. E. Gralinski, R. L. Graham, M. M. Becker, S. Tomar, T. D. Scobey, H. L. Osswald, A. Whitmore, R. Gopal, A. K. Ghosh, A. Mesecar, M. Zambon, M. Heise, M. R. Denison, R. S. Baric, A mouse model for Betacoronavirus subgroup 2c using a bat coronavirus strain HKU5 variant. *mBio*. **5**, e00047-00014 (2014).

40. S. E. St John, M. D. Therkelsen, P. R. Nyalapatla, H. L. Osswald, A. K. Ghosh, A. D. Mesecar, X-ray structure and inhibition of the feline infectious peritonitis virus 3C-like protease: Structural implications for drug design. *Bioorg. Med. Chem. Lett.* **25**, 5072–5077 (2015).

41. S. E. St John, B. J. Anson, A. D. Mesecar, X-Ray Structure and Inhibition of 3C-like Protease from Porcine Epidemic Diarrhea Virus. *Sci. Rep.* **6**, 25961 (2016).

42. X. Deng, S. E. StJohn, H. L. Osswald, A. O'Brien, B. S. Banach, K. Sleeman, A. K. Ghosh, A. D. Mesecar, S. C. Baker, Coronaviruses resistant to a 3C-like protease inhibitor are attenuated for replication and pathogenesis, revealing a low genetic barrier but high fitness cost of resistance. *J. Virol.* **88**, 11886–11898 (2014).

43. S. Tomar, Understanding the determinants for substrate recognition, regulation of enzymatic activity and the development of broad-spectrum inhibitors of coronavirus 3-chymotrypsin-like proteases Open Access Dissertations. https://docs.lib.purdue.edu/open_access_dissertations/1322, (2015).

44. Y.-C. Yen, A. M. Kammeyer, K. C. Jensen, J. Tirlangi, A. K. Ghosh, A. D. Mesecar, Development of an Efficient Enzyme Production and Structure-Based Discovery Platform for BACE1 Inhibitors. *Biochemistry*. **58**, 4424–4435 (2019).

45. A. Ianevski, L. He, T. Aittokallio, J. Tang, SynergyFinder: a web application for analyzing drug combination dose-response matrix data. *Bioinforma. Oxf. Engl.* **33**, 2413–2415 (2017).

46. M. A. Bakowski, N. Beutler, E. Chen, T.-T. H. Nguyen, M. G. Kirkpatrick, M. Parren, L. Yang, J. Ricketts, A. K. Gupta, M. V. Hull, P. G. Schultz, D. R. Burton, A. K. Chatterjee, C. W. McNamara, T. F. Rogers, *bioRxiv*, in press, doi:10.1101/2020.06.16.153403.

47. D. Stopher, S. McClean, An improved method for the determination of distribution coefficients. *J. Pharm. Pharmacol.* **42**, 144 (1990).

48. Z. Szakacs, G. Haegele, R. Tyka, 1H/31P NMR pH indicator series to eliminate the glass electrode in NMR spectroscopic pKa determinations. *Anal. Chim. Acta*. **522**, 247–258 (2004).

49. R. S. Obach, Prediction of human clearance of twenty-nine drugs from hepatic microsomal intrinsic clearance data: an examination of in vitro half-life approach and nonspecific binding to microsomes. *Drug Metab. Dispos.* **27**, 1350–1359 (1999).

50. G. S. Walker, J. N. Bauman, T. F. Ryder, E. B. Smith, D. K. Spracklin, R. Scott Obach, Biosynthesis of drug metabolites and quantitation using NMR spectroscopy for use in pharmacologic and drug metabolism studies. *Drug Metab. Dispos.* **42**, 1627–1639, 13 pp. (2014).

51. P. Yates, H. Eng, L. Di, R. S. Obach, Statistical methods for analysis of time-dependent inhibition of cytochrome P450 enzymes. *Drug Metab. Dispos.* **40**, 2289–2296 (2012).

52. J. C. Kalvass, T. S. Maurer, G. M. Pollack, Use of plasma and brain unbound fractions to assess the extent of brain distribution of 34 drugs: comparison of unbound concentration ratios to in vivo P-glycoprotein efflux ratios. *Drug Metab. Dispos.* **35**, 660–666 (2007).

53. Z. Yang, in *Drug Metabolism Handbook* (John Wiley & Sons, Ltd, 2008; https://onlinelibrary.wiley.com/doi/abs/10.1002/9780470439265.ch4), pp. 41–64.

54. M. Jamei, S. Marciniak, K. Feng, A. Barnett, G. Tucker, A. Rostami-Hodjegan, The Simcyp Population-based ADME Simulator. *Expert Opin. Drug Metab. Toxicol.* **5**, 211–223 (2009).

55. "Guidance for Industry Antiviral Product Development - Conducting and Submitting Virology Studies to the Agency" (FDA, 2006), (available at https://www.fda.gov/media/71223/download).

56. H. Mo, C. Yang, K. Wang, Y. Wang, M. Huang, B. Murray, X. Qi, S.-C. Sun, M. Deshpande, G. Rhodes, M. D. Miller, Estimation of inhibitory quotient using a comparative equilibrium dialysis assay for prediction of viral response to hepatitis C virus inhibitors. *J. Viral Hepat.* **18**, 338–348 (2011).

57. X. Duval, C. Lamotte, E. Race, D. Descamps, F. Damond, F. Clavel, C. Leport, G. Peytavin, J.-L. Vilde, Amprenavir Inhibitory Quotient and Virological Response in Human Immunodeficiency Virus-Infected Patients on an Amprenavir-Containing Salvage Regimen without or with Ritonavir. *Antimicrob. Agents Chemother.* **46**, 570–574 (2002).

58. L. Shen, S. A. Rabi, A. R. Sedaghat, L. Shan, J. Lai, S. Xing, R. F. Siliciano, A Critical Subset Model Provides a Conceptual Basis for the High Antiviral Activity of Major HIV Drugs. *Sci. Transl. Med.* **3**, 91ra63-91ra63 (2011).

59. M. H. L. Green, W. J. Muriel, Mutagen testing using TRP+ reversion in Escherichia coli. *Mutat. Res.* **38**, 3–32 (1976).

60. D. M. Maron, B. N. Ames, Revised methods for the Salmonella mutagenicity test. *Mutat. Res. Environ. Mutagen. Relat. Subj.* **113**, 173–215 (1983).

61. "OECD Guideline 471 (Genetic Toxicology: Bacterial Reverse Mutation Test)" (Ninth addendum, 21 Jul y1997).

62. W. S. Redfern, L. Carlsson, A. S. Davis, W. G. Lynch, I. MacKenzie, S. Palethorpe, P. K. S. Siegl, I. Strang, A. T. Sullivan, R. Wallis, A. J. Camm, T. G. Hammond, Relationships between preclinical cardiac electrophysiology, clinical QT interval prolongation and torsade de pointes for a broad range of drugs: evidence for a provisional safety margin in drug development. *Cardiovasc. Res.* **58**, 32–45 (2003).

63. A. M. Brown, D. Rampe, Drug-induced long QT syndrome: is HERG the root of all evil. *Pharm. News*. **7**, 15–20 (2000).

64. J. Weirich, H. Antoni, Rate-dependence of antiarrhythmic and proarrhythmic properties of class I and class III antiarrhythmic drugs. *Basic Res. Cardiol.* **93**, 125–132 (1998).

65. Y. G. Yap, A. J. Camm, Arrhythmogenic mechanisms of non-sedating antihistamines. *Clin. Exp. Allergy*. **29**, 174–181 (1999).

Acknowledgments: The authors would like to thank Sarah Lazzaro, Sumathy Mathialagan, Sangwoo Ryu, Mark West and Emi Yamaguchi (Pfizer) for the transporter inhibition studies. Angela Doran, Chad Limanni, Amanda Plante and Jocelyn Rosado for their in vivo and PK study support (Pfizer). Marcus Ewing (Pfizer) and Gail Johnson (Pfizer) for preformulation studies. Li

Hao (Pfizer) for sequence analysis support. Shinji Yamazaki (Pfizer) for PBPK modeling simulations. Daniel Lettiere, Michael Homiski, Michelle Kenyon, Asser Bassyouni, Declan Flynn, William Reagan, Victoria Markiewicz and Stephen Jenkinson for overseeing safety studies, and William Reagan, Shirai Norimitsu for expert clinical pathology and pathology support for the toxicology studies. Stephen Mason (Pfizer) for critical review and editorial input. Deli Huang for supplying the HeLa-ACE2 stably transfected cell line.

Funding: A.D.M acknowledges partial support for this project from federal funds from the National Institute of Allergy and Infectious Diseases, National Institutes of Health, Department of Health and Human Services, under Contract No. HHSN272201700060C. The content is solely the responsibility of the authors and does not necessarily represent the official views of the National Institutes of Health. The study performed in Dr. Jun Wang's laboratory is partially supported by NIH grant (AI147325) and the Young Investigator Award grant from the Arizona Biomedical Research Centre (ADHS18-198859). Scripps work was supported by a grant from the Bill & Melinda Gates Foundation #OPP1107194, and the Scripps Family Impact Fund of the Miramar Charitable Foundation (MCF) **Author contributions**: A.D.M, E.L and B.A contributed to conceptualization, investigation, analysis, visualization and data curation of inhibition of protease activity against a panel of coronavirus 3CLpro experiments . A.D.M contributed to funding acquisition, supervision, project administration and resources of these experiments. J.W and C.M contributed to conceptualization, investigation, analysis, visualization and data curation of the thermal shift experiments. JW contributed to funding acquisition, supervision, project administration and resources of these experiments. M.A.B, T.F.G supervised, designed and carried out antiviral synergy infection experiments. N.B, M.G.K and E.C contributed to the

generation of *in vitro* antiviral synergy data J.B, J.H, Y.Z, L.M.A, L.L,S.N, R.O, C.S, R.K, R.H and B.B contributed to the analysis, interpretation of protease and antiviral data from collaborators and internal data. E.K designed and interpreted the ADME transporter experiments, R.S.O, H.E, R.M.J, E.P.K contributed to the metabolism, pharmacokinetics and bioanalysis of PF-07304814 and PF-00835231. J.R.L, S.A.L, M.N.O., and M.T. designed and interpreted formulation experiments and characterization of API properties. M.R.R, M.P, K.O, R.H and D.O designed and synthesized PF-07304814. R.M.J, B.B, R.S.O and E.K contributed to the conceptualization, analysis and calculations for the prediction of human PK and dose estimate for PF-07304814. J.G.S, L.W.U, R.M.J contributed to the design, supervision and interpretation of in vitro and in vivo safety study data. C.A, A.A, M.I.R contributed to the scientific discussion, experimental design, data interpretation in addition to manuscript review and editing. All authors contributed to writing drafts of the manuscript. **Competing interests**: A.D.M has a sponsored program contract with Pfizer to test compounds for inhibition of coronavirus proteases. JW has a sponsored research agreement with Pfizer to test compounds for inhibition of coronavirus proteases. **Data and materials availability**: All data are available in the main text or the supplementary materials.

List of Supplementary Materials

Materials and Methods

Figures S1-S2

Tables S1-S11

References (34-65)

Table 1. Activity of PF-00835231 against 3CLpro of coronaviruses

Virus	**K_i (nM)**
Alpha-CoV	
NL63-CoV	0.77 ± 0.52
HCoV-229E	1.5 ± 0.76
PEDV	0.30 ± 0.11
FIPV	0.12 ± 0.10
Beta-CoV	
SARS-CoV-2*	0.27 ± 0.1
HKU1-CoV	0.85 ± 0.24
HKU4-CoV	0.034 ± 0.079
HKU5-CoV	0.033 ± 0.12
HKU9-CoV	0.74 ± 0.68
MHV-CoV	1.2 ± 0.90
OC43-CoV	0.51 ± 0.12
Gamma-CoV	
IBV-CoV	4.0 ± 0.37

*Data reported in (*15*)

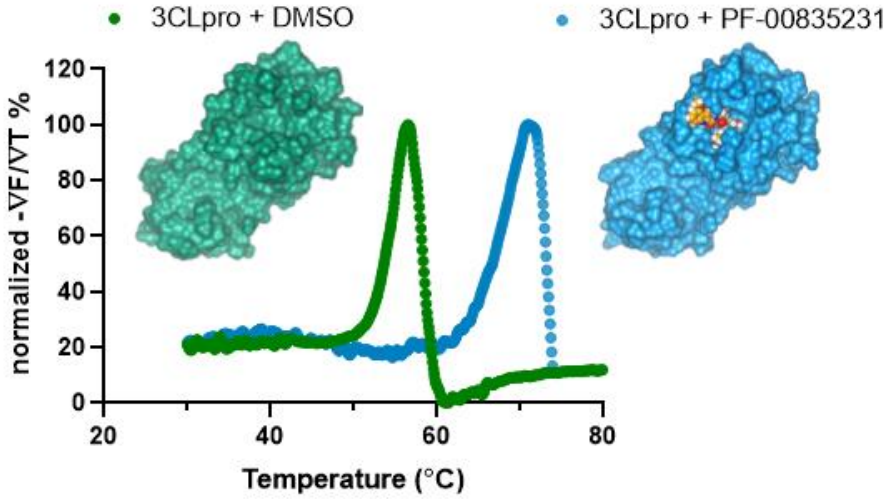

Fig. 1. Representative thermal shift binding data of PF-00835231 with SARS-CoV-2 3CLpro. X-ray structures of SARS CoV-2 3CLpro apoenzyme (left) and SARS CoV-2 3CLpro in complex with PF-00835231 (right).

A

Cells	Virus	P-gp Efflux Inhibitor	PF-00835231		PF-07304814	
			EC_{50} µM GeoMean (95% CI)	**CC_{50} µM** GeoMean (95% CI)	**EC_{50} µM** GeoMean (95% CI)	**CC_{50} µM** GeoMean (95% CI)
Vero E6-enACE2 (kidney)	SARS2 Washington 1	0	40 (30,53) n=10	>100 (ND) n=9	87 (71,110) n=10	>100 (ND) n=8
		0.5 µm	3.0 (1.1,7.7) n=7	>100 (ND) n=6	27 (7.6,94) n=7	>100 (ND) n=7
		2 µm	0.24 (0.14,0.41) n=6	>100 (ND) n=6	3.8 (1.6,8.8) n=7	>100 (ND) n=6
VeroE6-EGFP (kidney)	SARS2 BetaCov GHB-03021/2020	0	89 (77,100) n=5	>100 (ND) n=8	>50 (ND) n=4	>50 (ND) n=4
		0.5 µm	8.2 (3.1, 22) n=8	>100 (ND) n=8	27 (6.3, 120) n=2	>50 (ND) n=4
		2 µm	0.76 (0.45,1.3) n=4	>50 (ND) n=4	0.83 (0.50,1.4) n=3	>50 (ND) n=4
MRC-5 (lung)	HCoV-229E	0	0.069 (0.056,0.085) n=7	>100 n=5	0.074 (0.013, 0.42) n=3	>100 n=3
		0.5 µm	0.080 (0.017, 0.37) n=3	>100 n=3	0.058 (0.023, 0.15) n=3	>100 n=3

B

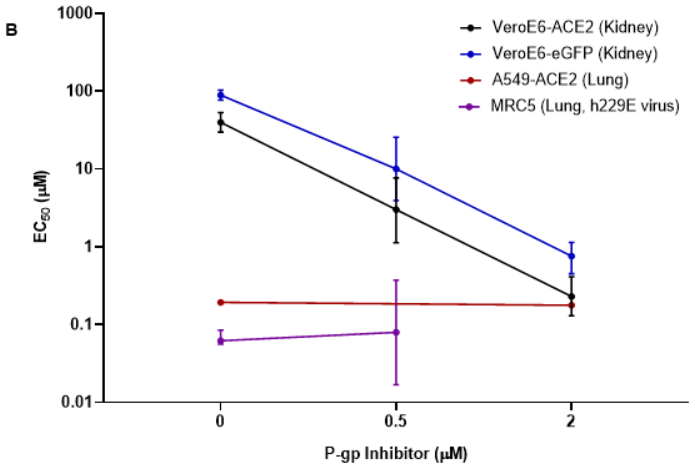

Fig. 2. Antiviral activity across cell lines and viruses. (**A**) *In vitro* antiviral activity, and cytotoxicity for PF-00835231 and PF-07304814 with and without the P-gp efflux inhibitor, CP-100356. (**B**) EC_{50} values with PF-00835231 with increasing P-gp inhibitor in human lung and monkey kidney cell lines. A549-ACE2 human lung carcinoma data (red) as reported in (*23*).

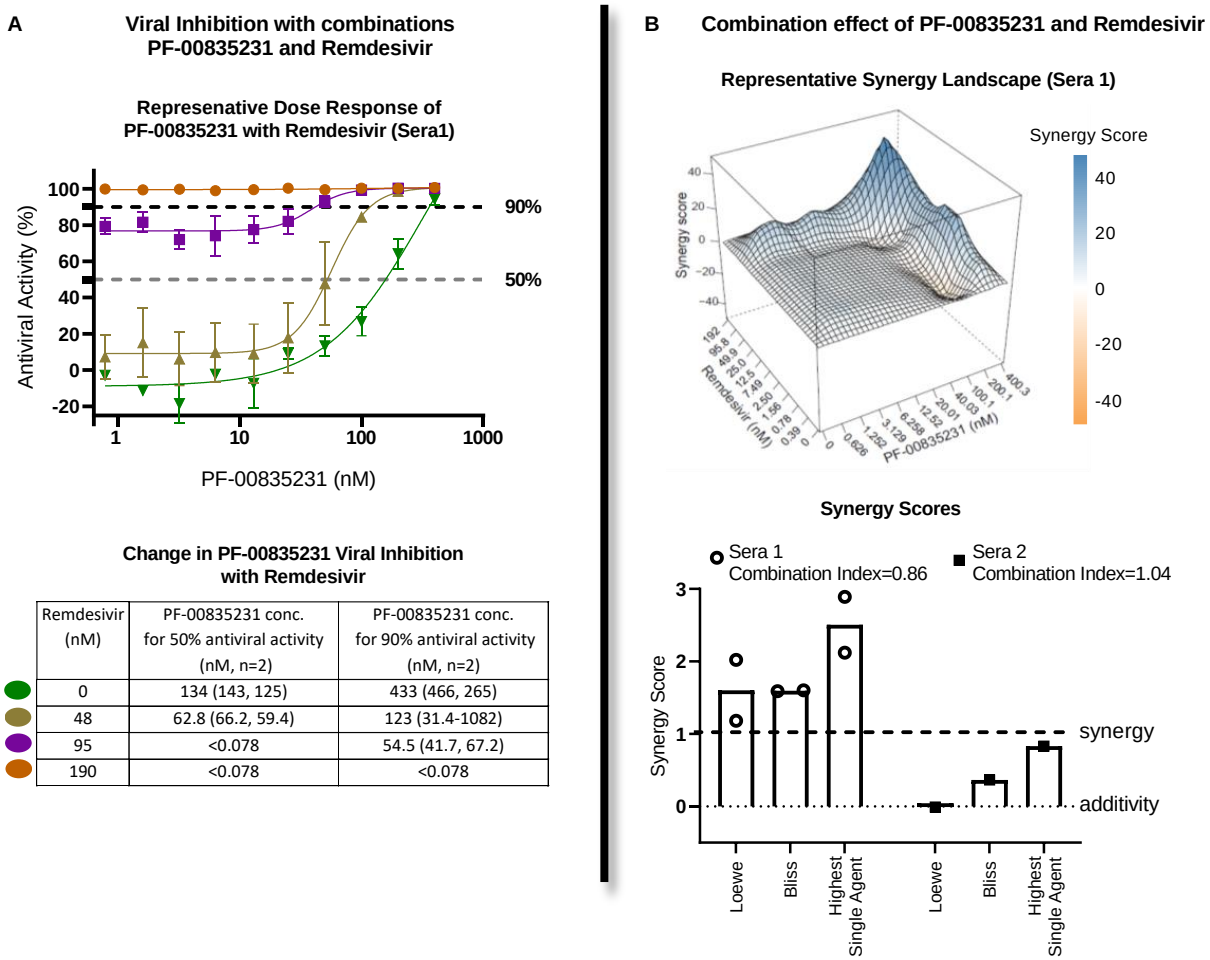

Remdesivir (nM)	PF-00835231 conc. for 50% antiviral activity (nM, n=2)	PF-00835231 conc. for 90% antiviral activity (nM, n=2)
0	134 (143, 125)	433 (466, 265)
48	62.8 (66.2, 59.4)	123 (31.4-1082)
95	<0.078	54.5 (41.7, 67.2)
190	<0.078	<0.078

Fig. 3. Measuring potential synergy between PF-00835231 and remdesivir in HeLa-ACE2 cells. (**A**) (Top) Representative antiviral dose response curves of PF-00835231 in combination with remdesivir against SARS-CoV-2. Serial dilutions of PF-00835231 with a range of fixed concentration of remdesivir. (Bottom) *In vitro* absolute antiviral activity shift in 50% and 90% antiviral activity with fixed concentrations of remdesivir. (**B**) (Top) A representative 3-dimensional drug interaction landscape plotting synergy scores analyzed using Synergyfinder (median scores of 3 replicates). (Bottom) Average *in vitro* combination synergy scores from the 3 experiments using 2 different patients' sera (shown separately).

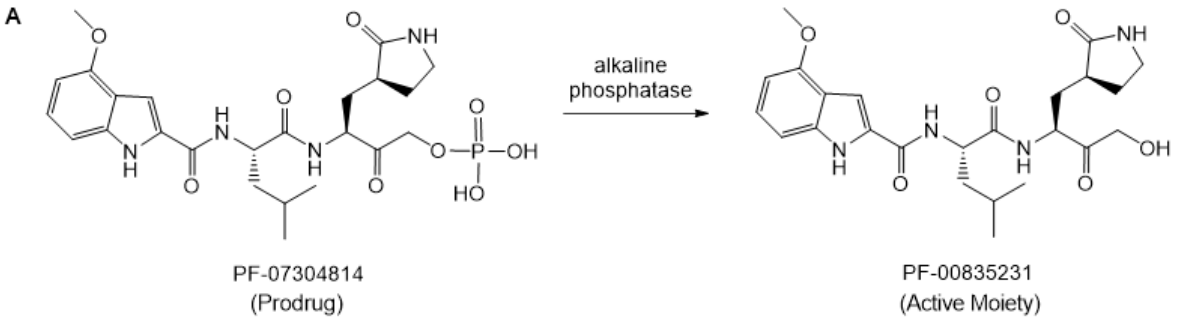

B

Dose Feasibility Matrix

	Solubility	Clinical Exposure (fold over EC90) 1x	3x	7x	10x
Aqueous solublity of PF-00835231	0.1mg/mL				
Feasible clinical formulation of PF-00835231 solubility	0.5mg/mL				
Aqueous solublility of PF-07304814 (Prodrug)	200 mg/mL				

Infeasible

Feasible with a Cyp3A inhibitor

Feasible

Fig. 4. PF-7304814 prodrug and PF-00835231 structures and dose considerations. (**A**) Chemical structure of conversion of prodrug PF-07304814 to the active moiety and PF-00835231 by alkaline phosphatase. (**B)** Dose feasibility matrix illustrating the ability to achieve higher target exposures with increasing solubility and the limitations of dosing PF-00835231. with dosing either aqueous PF-00835231, clinically formulated PF-00835231, or aqueous PF-07304814 (prodrug). The infeasible limit (red) is assumed to be 1 L per day with a 2x potential benefit with a Cyp inhibitor (orange). Any dose under that is considered feasible (green).

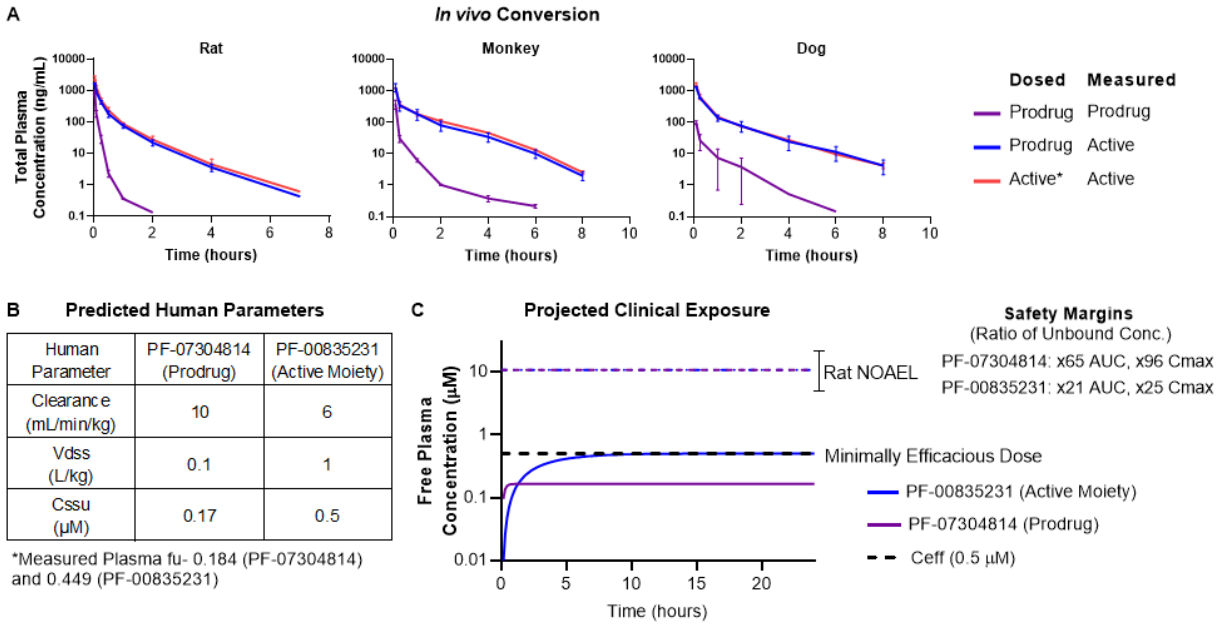

Fig. 5. PF-07304814 (prodrug) and PF-00835231 *in vivo* exposure summary. (**A**) Rat, dog and monkey PK following administration of PF-07304814 or PF-00835231 demonstrating high levels of PF-00835231 formed following administration of PF-07304814. (**B**) Predicted human PK parameters and measured protein binding for PF-07304814 and PF-00835231 used for human dose prediction. (**C**) Projected human systemic exposure profiles at the minimally efficacious dose of 500mg/day of PF-07304814 delivered as a continuous IV infusion. The predicted unbound steady state concentrations for the prodrug PF-07304814 (purple) and the active moiety PF-00835231 (blue) are 0.17µM and 0.5µM respectively.